

# Core-sheath Electrospinning of Shea Butter and Cellulose Acetate to Enhance Heat Transfer in Protective Clothing

**Hye Jin Kim**

Ewha Womans University

**Ji Hun Park**

Ewha Womans University

**Syifa Salsabila**

Seoul National University

**Changsang Yun** (✉ [cyun@ewha.ac.kr](mailto:cyun@ewha.ac.kr))

Ewha Womans University

---

## Research Article

**Keywords:** electrospinning, cellulose acetate, phase change material, heat transfer, skin temperature, protective clothing

**Posted Date:** November 29th, 2021

**DOI:** <https://doi.org/10.21203/rs.3.rs-978565/v1>

**License:**  This work is licensed under a Creative Commons Attribution 4.0 International License.

[Read Full License](#)

---

# 1 **Core-sheath electrospinning of shea butter and** 2 **cellulose acetate to enhance heat transfer in** 3 **protective clothing**

## 4 **Abstract**

5 Protective clothing for health workers requires heat transfer in hot and humid  
6 environments. To study the thermal conduction of phase-change materials and protect them from  
7 leakage, we selected skin-friendly shea-butter due to its suitable melting temperature, and the  
8 electrospinning processibility of biocompatible cellulose acetate. The shea-butter as a phase-  
9 change material was encapsulated in electrospun cellulose acetate fibres within a core/sheath  
10 structure, which was stabilised by two concentric Taylor cones during coaxial electrospinning.  
11 Transmission and scanning electron microscopy revealed a blood-in-tube vessel-like morphology.  
12 Next, differential scanning calorimetry and thermogravimetric analyses confirmed the heat  
13 capacity of shea-butter (latent heat of fusion: 42.73 J/g; thermal conductivity: 1.407 W/m·K). The  
14 flow rate of the core was proportional to the heat capacity of the shea-butter/cellulose  
15 fibres. This was consistent with the finding that the electrospun fibres of the highest-ratio shea-  
16 butter (16.19%) had the highest thermal conductivity (0.421 J/g·K). The shea-butter:cellulose  
17 acetate ratio was approximately 15:80. The efficacy of heat transfer for the core/sheath fibres in  
18 human clothing was assessed by measuring skin temperatures at 13 sites in six males aged 25 to 35  
19 under two conditions: wearing a mask and hood with attached cellulose acetate fibres in the  
20 presence and absence of shea-butter. The mean difference in skin temperatures (0.5 °C) between  
21 the two conditions was significant. Coaxial electrospinning of shea-butter/cellulose acetate fibres  
22 is therefore promising for protective clothing with efficient heat-transfer in the use of a large area.

## 23 *Keywords*

24 *electrospinning·cellulose acetate·phase change material·heat transfer·skin*  
25 *temperature·protective clothing*

## 26 **Abbreviations**

27 CA: cellulose acetate

28 PCM: phase change material

29 ShB: shea butter

30 CCN: coconut oil

31 C/S: CCN/ShB 1:1 (wt%)

32 A: acetone

33 D, DMF: dimethyl formamide

34 TiO<sub>2</sub>: titanium oxide

- 35 ZnO: zinc oxide  
36  $T_m$ : melting temperature  
37  $T_c$ : solidifying (crystallising) temperature  
38  $\Delta H$ : latent heat of fusion (enthalpy)  
39  $C_p$ : specific heat of at constant pressure  
40  $k$ : thermal conductivity  
41

## 42 **Introduction**

### 43 *Protective clothing for COVID-19 medical workers in hot-humid environments*

44 Demand is growing for smart clothing and textiles that can protect wearers working in  
45 hot, humid environments by means of an integrated cooling mechanism. Due to the coronavirus  
46 disease 2019 (COVID-19) pandemic, protective clothing has become essential for both patients  
47 and medical personnel. Because the COVID-19 virus can be spread through inhalation of droplets  
48 and aerosols, healthcare workers are required to cover their respiratory organs. Unfortunately,  
49 wearing coveralls, medical gowns, N95 and filtering face masks, goggles, gloves, and powered air-  
50 purifying respirators for extended periods can result in heat strain and thermal discomfort (Park,  
51 2020). For prolonged wear, virus-protective clothing should provide thermal comfort as well as  
52 intrinsic protective functions.

53

### 54 *Electrospinning of cellulose acetate for protective clothing*

55 Textiles and other materials used in protective clothing are required to provide high levels  
56 of functionality, which can cause thermal discomfort, leading in turn to a need for clothing that can  
57 offer enhanced heat-transfer abilities. Although cellulose is one of the most abundant and skin-  
58 friendly of biomaterials, it is relatively vulnerable to cell propagation and cannot be easily  
59 fabricated by electrospinning because it is insoluble in moderate acids and solvents (Khalf *et al.*  
60 2015). Among cellulose derivatives, cellulose acetate (CA) is biodegradable and biocompatible  
61 and can be chemically processed with various solvents to fabricate electrospun fibres with a wide  
62 variety of applications, including separation membranes, tissue engineering, sensors, and catalysts  
63 (Aboamera *et al.* 2018; Liebert 2010; Wang *et al.* 2020; Zhang *et al.* 2018). Because  
64 electrospinning produces fibres with a high volume to specific-surface-area ratio, electrospun CA  
65 can intensify cell attachment, corresponding to an increase in pore number and sizes (Khalf *et al.*  
66 2015). However, the microbial susceptibility of CA fabric needs to incorporate antibacterial  
67 nanoparticles. According to Anitha *et al.* (2013), Jatoi *et al.* (2020), and Phan *et al.* (2019),  
68 antimicrobial CA can be fabricated by inserting zinc oxide, copper, or silver nanoparticles in  
69 combination with thermo-conductive or thermo-regulative fillers, carbonaceous materials, or fatty  
70 oils. Table 1 lists previous reports that explore the functional results of electrospinning CA with  
71 nanoparticle additives. Electrospun CA with bactericidal additives appears to be suitable for  
72 protective and comfortable respiratory masks that can effectively transfer heat.

73

74 *Thermal conductivity of phase-change materials*

75 To enhance thermal comfort through thermal conductivity ( $k$ ) mechanisms, phase-change  
76 materials (PCM) can be applied to the fabrication of protective face masks. The ideal PCM  
77 requires a melting point ( $T_m$ ) range appropriate for its application; sufficient latent heat of fusion  
78 ( $\Delta H$ ); sufficient specific heat ( $C_p$ ) capacity; a small change in phase volume; the absence of  
79 supercooling; chemical stability; high resistance to flammability, explosion, and toxicity; and high  
80 resistance to corrosion of the sheath materials. Such a material must also be easily processed and  
81 available at acceptable costs and quantities, according to Abhat 1983, Shchukina *et al.* 2018,  
82 Udangawa *et al.* 2019. Among the four types of PCMs (solid-liquid, solid-solid, solid-gas, and  
83 liquid-gas), solid-liquid PCMs offer higher  $\Delta H$  and smaller changes in volume compared with  
84 solid-solid and solid-gas PCMs, making them suitable for thermal energy storage (Shchukina *et al.*  
85 2018). Solid-liquid PCMs are available in organic, inorganic, and eutectic varieties. While an  
86 inorganic PCM of hydrated salts has a high  $\Delta H$  per volume (250 to 400 J·dm<sup>-3</sup>) and  $k$ , organic  
87 PCMs of paraffin wax, fatty acids, and polyethylene glycol are favourable in terms of congruent  
88 melting without kinetically supercooling (Abhat 1983; Hemmatian *et al.* 2020; Oh *et al.* 2020).  
89 The  $n$ -alkane chains of paraffin wax affect the phase transition between an isotropic liquid and a  
90 well-ordered crystal. In this “metastable rotator phase”, the number of carbon atoms (20 to 40) is  
91 related to the  $T_m$  of paraffin PCM and its  $\Delta H$  (Sharma *et al.* 2015; Cholakova and Denkov, 2019).  
92 Meanwhile, fatty-acid PCMs consist of an aliphatic chain of 13 to 21 carbon atoms, the length of  
93 which is proportional to the weight percentage of the fatty acid and the number of carbon atoms,  
94 with a carboxyl group and a methyl group at each end (Wahyudi *et al.* 2018). Floros and Narine  
95 (2016) reported that diesters from fatty acids produced  $\Delta H$  of 230 to 260 J·g<sup>-1</sup>, which were higher  
96 than  $\Delta H$  of paraffins (150 to 200 J·g<sup>-1</sup>), with  $T_m$  of between 39 °C and 77 °C produced by reacting  
97 dialcohols with methyl esters.

98 A fatty-acid methyl ester from lipids is non-toxic, environmentally friendly, renewable,  
99 bactericidal, and safe for human skin, making it suitable for PCMs. Some fatty acids of PCMs  
100 exhibit phase transition near skin temperatures, ranging from 28 °C to 35 °C (Sharma *et al.* 2015).  
101 One such fatty acid, shea butter, has a  $T_m$  of 32 °C to 45 °C, which is higher than that of coconut  
102 oil (21 °C to 25 °C). This can be attributed to the longer chains of the main components of shea  
103 butter: stearic acid (41.8%) and oleic acid (46.5%) (Table 2), offsetting the higher  $T_m$  of stearic  
104 acid (69 °C) with that of oleic acid (16.3 °C), according to Udangawa *et al.* (2019), Eckey (1954)  
105 and Leakey (1999). The primary constituent of coconut oil, at 52.0% to 53.2%, is lauric acid  
106 (C<sub>12</sub>H<sub>24</sub>O<sub>2</sub>), the  $T_m$  of which is 43.2 °C. Other components include 16.8% to 21.0% myristic acid  
107 (C<sub>14</sub>H<sub>28</sub>O<sub>2</sub>), 7.5% to 10.2% palmitic acid (C<sub>16</sub>H<sub>32</sub>O<sub>2</sub>), 5.0% to 10.0% oleic acid (C<sub>18</sub>H<sub>34</sub>O<sub>2</sub>), and  
108 2.0% to 4.0% stearic acid (C<sub>18</sub>H<sub>36</sub>O<sub>2</sub>). The flash and solidifying points of the shea butter are also  
109 higher (> 200 °C and 17 °C to 27 °C, respectively) than those of coconut oil (113 °C and 9% to  
110 16 °C, respectively). In short, shea butter (the eutectic of methyl stearate) offers a phase-change  
111 temperature closer to that of the human body temperature of 37.5 °C compared with coconut oil  
112 (the eutectic of methyl oleate).

113  
114

115 *Fabrication of core-sheath structural fibres using coaxial electrospinning*

116 Numerous techniques for inserting the inorganic materials have been investigated to  
117 enhance the thermal transfer capacity of PCMs. These techniques include ultra-sonification of sol-  
118 gels, vacuum impregnation, hydrothermal processes, and carbonization. Among the techniques,  
119 electrospinning in a core-sheath (core-shell) structure is a promising method of expanding the  
120 surfaces of PCMs (Ali *et al.* 2019; Song *et al.* 2019). The nano-scaled PCM capsules also exhibit  
121 relatively efficient  $k$  due to a large surface-area-to-volume ratio during electrospinning. (Salunkhe  
122 and Shembeker 2012). Cai *et al.* (2013) used electrospinning to manufacture a composite of  
123 overlaid polyamide-6 nanofibres with the eutectics of capric-lauric-palmitic-stearic acids, and the  
124 inclusion of 10 wt% expanded graphite induced the nanofibrous composite to absorb the acid  
125 eutectics, increasing heat enthalpy and thermal capacity. Chen *et al.* (2013) manufactured  
126 composite PCM electrospun fibres of polyethylene glycol-cellulose acetate as a core-sheath and  
127 found that the content of polyethylene glycol affected the enthalpy of phase change. Pittarate *et al.*  
128 (2011) added 9 wt% polyethylene oxide (PEO) to an electrospun nanocomposite of cellulose  
129 acetate to enhance its elastic modulus, elongation at break, and tensile strength by 253%, 54%, and  
130 446%, respectively. The low  $k$  of polymeric sheaths can be supplemented by the addition of  
131 inorganic materials such as expanded graphite, carbon nanotubes, GO, ZnO, or silica particles.  
132 Adding ZnO nanoparticles of 20 wt% of PEO maximised those values by 31%, 12%, and 47%,  
133 respectively, leading to a decrease in phase-change temperature by between  $-9^{\circ}\text{C}$  and  $1^{\circ}\text{C}$ .

134 The design of protective textiles and clothing in hot, humid environments requires  
135 wearing trials from the design stage. In such environments, body temperature and sweat are unable  
136 to circulate out of the textiles and clothing, which activates heat dissipation by the human body to  
137 improve thermal comfort through evaporation, convection, conduction, and radiation. Between the  
138 skin and the textiles, the human body constantly transfers heat and moisture to keep a comfortable  
139 state by controlling body and skin temperature through vaso-venodilation-constriction of arterial  
140 flows to hands and feet, and evaporation of perspiration (Caldwell *et al.* 2014). Bedek *et al.* (2011)  
141 reported that, when skin temperature was predicted in simulations, the temperature was affected  
142 primarily by the  $k$  of underwear, and skin humidity was related to evaporation resistance,  
143 absorption rate, and drying time. Ghaffari *et al.* (2019) studied moisture resistance, air  
144 permeability, thermal insulation, and the resulting thermal comfort of electrospun polyacrylonitrile  
145 fibres sandwiched between a plain polyester fabric and a nylon-warp knitted fabric. Raccuglia *et*  
146 *al.* (2017) evaluated the subjective perception of skin wetness, thermal sensation, and thermal  
147 comfort produced by 24 samples by applying them to the upper backs of 12 male and female  
148 subjects. The study revealed that thickness affected the perception of cooling sensation and  
149 humidity, and the cooling capacity was proportional to the moisture content of the fibres.

150 This study was designed to develop a cooling-functional textile by electrospinning  
151 encapsulated PCMs in CA in a core-sheath structure. One objective was to fabricate the  
152 electrospun shea butter-CA with encapsulating additives in an attempt to intensify the  $k$  of the  
153 sheath and latent heat, leading to solidification of the core. The other was to evaluate the actual  
154 thermal regulation by suppressing the increase in skin temperature of six subjects. The results of a  
155 human-wearing assessment are compared with those of thermophysical tests to evaluate the

156 practical heat-transfer performance of functional clothing for healthcare workers treating patients  
157 with COVID-19.

## 158 **Experimental methods**

### 159 *Materials*

160 Cellulose acetate with a degree of acetylation of  $55 \pm 3\%$  was obtained from Daejung  
161 Chemicals & Metals, Ltd and Kanto (Korea and Japan). Gel permeation chromatography revealed  
162 that CA had an average molecular weight ( $M_n$ ) of 139,000, a mass average molecular weight ( $M_w$ )  
163 of 270,000, and a polydispersity index of 1.94. As solvents, acetone 99.8%, dimethylformamide  
164 (N,N-Dimethylformamide [DMF]) were purchased from Daejung Chemicals & Metals, Ltd  
165 (Korea). As a PCM for this study, shea butter (*Butyrospermum parkii*) consisting of 41.8% stearic  
166 acid and 46.5% oleic acid, along with coconut oil were purchased from Kerfoot (UK) and Ottogi  
167 Co., Ltd. (Korea). To provide the electrospun core and sheaths with  $k$ , radiation protection, and  
168 antibacterial activity, three additives were used: aqueous graphene oxide (GO) (Uni-Nanotech  
169 Corp, Korea) containing approximately 80% graphene flakes at a concentration of 6.2 g/L and a  
170 flake size of 0.5 to 5  $\mu\text{m}$ , titanium dioxide ( $\text{TiO}_2$ ), and zinc oxide (ZnO) (Guwall cakesoap Ltd.,  
171 Korea).

172

### 173 *Preparation and electrospinning*

174 This study used a solvent system of acetone for electrospinning solutions: acetone with  
175 DMF at five different acetone:DMF (v/v) ratios (4:1, 2:1, 1:1, 1:2, 1:4). In the mixed solvents,  
176 electrospinning solutions of cellulose acetate were attempted at five concentrations between 17.5  
177 wt% and 27.5 wt% at intervals of 2.5 wt%. As shown in Fig. 1, the CA powder was mixed  
178 physically with additives equivalent to 5% of the acetate weight. The mixture of prepared powder  
179 was then poured into an Erlenmeyer flask and dissolved in the mixed solvents at 55 °C to 60 °C  
180 while strongly stirred by a magnetic stirrer. Following completion of the dissolution reaction, the  
181 prepared solution was injected into a 10 cc syringe, and air bubbles in the syringe were removed.

182 The electrospinning device (ESR200, eS-robot, NanoNC Ltd., Korea) comprised two  
183 pumps, a robot that moves the pumps along the x and y axes, and a rotary drum collector. This  
184 device provided high voltage up to 30 kV in an acrylic box. The tips of the dual nozzle used in  
185 coaxial spinning had an inner diameter of 1.23 mm and an outer diameter of 1.50 mm in size, and  
186 the inner and outer diameters of a core needle were 0.33 mm and 0.63 mm, respectively. The  
187 sheath solution from another syringe was injected into the tube connecting to the dual nozzle with  
188 polyethylene and polytetrafluoroethylene tubes measuring 1/16 and 3/32 inches in diameter,  
189 respectively. For comparison with the core-sheath electrospun fibres, the needle of a single nozzle  
190 for electrospinning CA fibres with an inner/outer diameter of 0.5 mm/0.8 mm, which is similar to  
191 the area of the sheath, was used. The flow rate varied from 0.1 to 7.0 mL/h, the distance from the  
192 tip to the collector (TCD) ranged from 5.5 to 15.0 cm, and the applied voltage was from 13 to 25  
193 kV. The final setting of core-sheath electrospinning was for the CA solution of 22.5 wt% to 25.0  
194 wt%. Electrospun fibres of the PCM-CA were collected by aluminium foil wrapped around a drum  
195 rotating at 250 rpm. In Table 3, all 22 electrospun specimens are classified according to the

196 presence or absence of PCMs or additives, the type of PCMs, concentration, volume ratio of the  
197 binary solvent systems, and the flow rate of core and sheath.

198

#### 199 *Electrospun-fibre observations*

200 Transmission electron microscopy (TEM), scanning electron microscopy (SEM), and  
201 optical microscopy of the electrospun fibres of core-sheath were used to confirm the presence of  
202 PCMs encapsulated in the CA sheath. During the experiments, the electrospun PCM-CA fibres  
203 were collected directly on 200-mesh copper grids coated with lacey carbon. Morphological images  
204 of the core-sheath fibres were taken using a field emission TEM (JEM-2100F, Joel Ltd.) at 200  
205 kV. High-resolution SEM (SU8220, Hitachi Ltd.) at the Seoul Western Centre, Korea Institute of  
206 Basic Science, was also used to image the PCM-CA fibres at voltages of 10 to 15 kV. The  
207 electrospun fibres were examined directly through an optical microscope (Eclipse LV100ND,  
208 Nikon). The diameter of fibres and fibrils in a total of 60 to 90 per case were measured using  
209 ImageJ (National Institutes of Health, USA) and Gryphax software (Jenoptik, Japan), and  
210 frequency analyses of the fibre and histograms of fibre-size distribution were conducted in SPSS  
211 19.0 (IBM SPSS Statistics).

212

#### 213 *Thermal characterization*

214 The latent heat of fusion and thermal weight loss of the electrospun PCM-CA fibres were  
215 measured through differential scanning calorimetric analysis (DSC) and thermogravimetric  
216 analysis (TGA). To compare the thermal capacity of PCM-CA fibres and PCM itself, the  
217 enthalpies and melting-freezing peaks of each sample were analysed with a DSC (DSC 25, TA  
218 Instruments). The DSC measurement went through each stage at a nitrogen atmosphere as follows.  
219 First, 10 mg of each sample was placed in a Tzero aluminium pan. Next, the samples were  
220 stabilised at 25°C in an isothermal state for 1 min. They were then heated to 50°C at a rate of  
221 10°C/min, isothermalised for 1 min, and then cooled to -10 °C at 20 °C/min, after which they  
222 stayed in an isothermal state for 1 min. For the second heating-cooling cycle, they were reheated  
223 and recooled to between -10 °C and 50 °C, and each stage was accompanied by isothermalising  
224 for 1 min. For TGA measurements, Q50 and Discovery (TA Instruments) devices were used. A  
225 platinum pan was weighed without any sample and after each sample was contained, and the  
226 samples were then heated from 25 °C to between 600 °C and 800 °C at a rate of 10 °C/min in a  
227 nitrogen atmosphere.

228

#### 229 *Application to facial mask hoods through 3D scanning and 3D printing*

230 A face hood was fabricated to attach the PCM-CA electrospun fibres. The hood had to be  
231 stuck to the subjects' skin to increase the  $k$  of the PCM. To ensure an ergonomic design of the face  
232 hood, 3D scanning of a single adult male in his early 30s was performed from the head to the  
233 shoulder, and the left figure of the scanned face and head was symmetrically modelled in CAD  
234 software (Rhino 7, Robert McNeel & Associates) to create a human body model. This model was  
235 3D-printed at full size with polylactic acid filaments using an FDM-type printer (Replicator+,  
236 MakerBot). The model was sliced into eight parts according to the size of the printer. The printing  
237 time for each part was 20 to 26 hours, with a total print time of eight days. The divided output was

238 finished by bonding with putty, bond, and carboxymethyl cellulose. The pattern of the face hood  
239 was draped with line-tape on the finished model. A 95%/5% polyester/polyurethane composition  
240 was used for the face hood fabricated by 3D draping on a model made by 3D scanning and 3D  
241 printing.

242

#### 243 *Human-wearing assessment*

244 Six healthy male subjects aged 25 to 32 years were recruited by distributing recruitment  
245 documents at sports centres and health clubs for 10 weeks or through expert recommendations,  
246 with the approval of Ewha Womans University Institutional Review Board (No: ewha-202010-  
247 0014-03). After receiving sufficient explanation and signing the consent form, the subjects  
248 measured their height, weight, heart rate, and pulse rate (an average height of  $175.01 \pm 4.61$  cm, an  
249 average weight of  $76.93 \pm 8.58$  kg, and average body mass index of  $25.12 \pm 2.60$ ). For each  
250 subject, 13 skin temperatures and left auditory canal temperatures were measured, including two  
251 facial body parts (left temple, left cheek), five upper-body parts (front neck, chest, upper left arm,  
252 lower left arm, and left hand), and five lower-body parts (abdomen, waist, left thigh, left calf, and  
253 left foot). A set of 8-channel thermistors (Gram LT-8A, Japan) were simultaneously used as skin-  
254 temperature sensors, and infrared thermography was taken with a thermal imaging camera (Flir  
255 C3, USA). An artificial climate room was set at  $33.0$  °C,  $70 \pm 2\%$  relative humidity.

256 This study collected a total 13 skin-temperature records of the six subjects. To calculate  
257 the mean skin temperature of each subject, the Hardy and Dubois formula was used as follows:

258 Mean skin temperatures (seven-point method)

$$\begin{aligned} 259 \quad &= 0.07 * T_{\text{forehead}} + 0.35 * T_{\text{chest}} + 0.14 * T_{\text{arm}} + 0.19 * T_{\text{thigh}} \\ 260 \quad &+ 0.13 * T_{\text{calf}} + 0.05 * T_{\text{hand}} + 0.07 * T_{\text{foot}} \quad \text{Eq.(1)} \end{aligned}$$

261 Mean skin temperatures, auditory canal temperatures and subjective perception records  
262 were obtained from the human-wearing evaluation and analysed statistically using SPSS 19.0. The  
263 two experimental conditions of six subjects depended on the presence or absence of PCM: one  
264 conditioned for attaching the CA samples containing PCMs and the other for attaching the CA  
265 samples without PCMs. A paired-sample t-test was used to analyse the difference in the two  
266 conditions to confirm the effect of PCM fibres attached to the hoods on mean skin temperature ( $p$   
267  $< 0.05$ , two-way t-test).

## 268 **Results and discussion**

### 269 *Monoaxially electrospun CA as a sheath and coaxially electrospun PCM as a core*

270 The morphology of the electrospun cellulose acetate CA fibres was examined with a  
271 single nozzle and the PCM-encapsulating CA fibres were examined with a double nozzle through  
272 optical microscopy, SEM, and TEM. The diameters of the fibres and fibrils and the thickness and  
273 weight of the electrospun fibres were also measured. To select a suitable solvent for the CA  
274 solution, the solubility of CA and the solvents was considered with Hansen solubility parameters  
275 (HSPs). Water ( $\delta_T$ : 48.18~47.90 MPa<sup>0.5</sup>) is a non-solvent of CA ( $\delta_T$ : 19.89 MPa<sup>0.5</sup>;  $\delta_H$ : 11.10  
276 MPa<sup>0.5</sup>) that does not enter within the radius of the HSPs. DMF ( $\delta_H$ : 11.30 MPa<sup>0.5</sup>) exhibit superior

277 solubility compared with acetone ( $\delta_h$ : 6.97 MPa<sup>0.5</sup>). The concentration of the solution dissolved  
278 with DMF wt% was much higher than that of the solution (below 15 wt%) when CA was  
279 dissolved with 100% acetone as a single solvent (Tungprapa *et al.* 2007). Mixing soluble solvents  
280 with CA resulted in higher critical-chain entanglement and improved the electrospinnability of  
281 CA. Mixing volatile solvents such as acetone is also necessary as the nano-scaled, rod-shaped CA  
282 electrospun fibres were neatly solidified when the solvent was sufficiently volatilised during jet  
283 ejection. When the solubility of a solvent is too high, the viscoelasticity of the solution may be  
284 insufficient for electrospinning (Lee *et al.* 2018).

285 The surfaces of the CA fibres varied from smooth surfaces resembling vinyl films to  
286 rough surfaces with paper-like fibre grains when electrospun in various solvent ratios. This pattern  
287 changed considerably depending on the acetone ratio. The lower the acetone ratio and the higher  
288 the DMF ratio, the more the fibres agglomerated like a smooth vinyl film, which is consistent with  
289 the literature (Aboamera *et al.*, 2019; Crabbe-Mann *et al.* 2018). However, because other variables  
290 are involved in addition to the solvent ratio, dependence on the solvent ratio was not necessarily  
291 evident. In the A:D 4:1 solution, the acetone volatilised too quickly in a dry environment; it  
292 solidified before reaching the collector and was difficult to call an electrospun fibre. A mixed  
293 solvent ratio was therefore selected as A:D 1:1 instead of the high ratio of DMF at which the  
294 surface of the electrospun fibres had lost their cellulose properties and the low ratio of DMF when  
295 the surface was too dry and rough.

296 Electrospun CA fibres of 25 wt% at a ratio of A:D 1:1 had a tree-leaf shape and a  
297 diameter of 2.39 to 3.04  $\mu\text{m}$ . In Fig. 2 (a), the CA fibres electrospun from the single nozzle are  
298 characterised by a few transparent microfibrils shaped like midribs (approximately 100  $\mu\text{m}$ )  
299 penetrating straight and numerous nanofibrils resembling side veins (approximately 500 nm)  
300 intertwining with each other. The diameter of the electrospun CA fibres was bisected at the  
301 micrometer scale (with a maximum value 28.25 to 28.45  $\mu\text{m}$ ) and the nanometer scale (with a  
302 minimum value of 270 to 970 nm), offsetting the average diameter. This can be attributed to the  
303 high flow rate, which widened the distribution due to the large volume of solution, which was  
304 demanded for the shell used in coaxial electrospinning to embrace the relatively large PCM core.  
305 We inferred that the acetone and DMF solvents did not mix homogeneously but combined  
306 separately with the CA polymers. Alternatively, insufficient voltage or too great inflow rate may  
307 have made it impossible for the solution jet flown to the collector to split, causing colloidal  
308 aggregation of the molecular chains. Some electrospun CA fibres may have failed to overcome the  
309 surface tension of the solution at the tip and Coulomb repulsion in the jet stretching due to the  
310 positive charge that was dispersed from its TiO<sub>2</sub> and ZnO.

311 In coaxial electrospinning using the dual nozzle, we investigated the morphological  
312 characteristics of the encapsulation of shea butter (ShB) inside the CA sheath. As shown in Fig. 3  
313 (a), two concentric Taylor cones of each core and sheath solution were observed when the  
314 solutions were ejected from the tip of the dual nozzle. Due to Plateau-Rayleigh instability, the  
315 droplet of the spinning solution, originally spherical in shape due to surface tension, was stretched  
316 to an ellipse by jet stretching. Based on the TEM images in Fig. 3 (b) and (d), a cylindrical  
317 morphology with small beads characterised the core-sheath fibre, and ShB was inserted into the

318 CA fibres. However, when the flow rate of sheath did not correspond to that of core, some ShB  
319 leaked from the sheath, as shown in the left side the SEM image of Fig 3 (c). This may be  
320 attributable to the fact that the excessively high voltage applied to the dual nozzle split the ejected  
321 droplets.

322 Next, we investigated the effects of the core-sheath flow rate on the encapsulation of  
323 PCM in CA during core-sheath electrospinning. To determine the appropriate ratio for the sheath  
324 and the core, the inflow rate of the sheath was set from 1.0 mL/h to 8.0 mL/h, and the inflow rate  
325 of the core was set to 0.5 mL/h and 1.0 mL/h. In coaxial electrospinning, the viscosity of the core  
326 must be lower than that of the sheath, and the flow rate of the sheath must be sufficient to cover  
327 the core. The inflow rate set by the viscosity ratio between the core and the sheath is therefore  
328 critical (Khalf *et al.* 2015). For successful coaxial electrospinning, appropriate flow rates and  
329 voltage were required to keep two Taylor cones continuously stable and protect the core by the  
330 sheath against corrosion or fibre breakage. The encapsulated PCMs do not just protect the  
331 durability of the core and the stability of thermal cycling, but also augment multiple functions of  
332 its sheath by coating the surface of the PCM. The encapsulated PCM protects the core by avoiding  
333 leakage during thermal cycling and corrosion of or damage to its sheath (Alehosseini and Jafari  
334 2020). The cellulose sheaths encapsulating the PCMs, octadecane, or linseed oil by coating with  
335 polysiloxane resins also control insulation, and ultraviolet protection, and play roles in self-  
336 cleaning, and self-healing to reinforce protective textiles or clothing (Li *et al.* 2019; Chen *et al.*  
337 2020).

338

### 339 *Heat transmittance of electro-spun fibres in DSC and TGA analysis*

340 To study the effect of sheath flow rate on the  $k$  of the PCM-CA fibre, we analysed eight  
341 specimens, including ShB itself, with DSC and TGA. Table 4 and Fig. 4 illustrate the kinetic,  
342 thermophysical, thermodynamic characteristics of seven ShB-CA electrospun fibres, coconut oil,  
343 and ShB as revealed by DSC. As the main PCM in this study, ShB melted from 32.06 °C and  
344 reached its maximum at 37.86 °C with an enthalpy of 42.73 J·g<sup>-1</sup>. When crystallised, the phase  
345 change from liquid to solid began at 13.49 °C, and its peak was reached at approximately 6.00 °C  
346 to 8.79 °C. When the temperature increased in the second heating step, ShB began to melt at a  
347 temperature that was half that of the initial  $T_m$  (about 15 °C) to approximately half the enthalpy  
348 (21.368 J·g<sup>-1</sup>), and the temperature at the third heating-cooling cycle showed almost the same  
349 pattern as the second. This could be due to lack of crystallisation time, as it took at least 20 min to  
350 fulfil its own thermal function. Coconut oil had a  $T_m$  of 30.27 °C ( $T_{m\text{ onset}}$ : 25.70 °C) and a  
351 solidification peak at 2.14 °C ( $T_{c\text{ onset}}$ : 4.54 °C). This shows that, because ShB (at 37.86 °C) was  
352 closer to body temperature than coconut oil (at 30.27 °C), ShB could meet the first ideal PCM  
353 requirement, the proper range of  $T_m$  for its application (Abhat 1983, Shchukina *et al.* 2018,  
354 Udangawa *et al.* 2019).

355 Despite the ideal melting temperature, whether the thermophysical characteristics of ShB  
356 are adequate for the effective PCMs should be considered in association with the fatty-acid content  
357 and latent heat, as well as congruent behaviours of melting and crystallisation. Lawer-Yolar *et al.*  
358 (2019) pointed out that ShB was appropriate for thermal energy storage but inappropriate for a

359 PCM because its  $T_m$  (4.3 °C to 15.8 °C) was broader and its  $\Delta H$  during freezing (29.9 to 41.6 J·g<sup>-1</sup>)  
 360 <sup>1</sup>) was lower than those of palm kernel oil and Allanblackia oil. Their result of the  $T_m$  was quite  
 361 different from that of shown in Table 2 (Lawer-Yolar *et al.* 2019; Canale *et al.* 2005), because the  
 362 ShB in their study comprised the different content of a lower stearic acid (least 20%) and a higher  
 363 mono-unsaturated oleic acid (up to 60%). The feasibility of stearate in ShB for PCMs was  
 364 confirmed in studies of methyl palmitate:methyl stearate at a 4:1 ratio, the synthesis of stearic acid  
 365 into a porous carbonised-maize straw matrix by vacuum impregnating, and a eutectic mixture of  
 366 stearic acid and benzamide s of 65.9 °C and  $\Delta H$  of 200.15 J·g<sup>-1</sup> due to added graphite that boosted  
 367  $k$  (Feldman *et al.* 1993; Suppes *et al.* 2003; Wen *et al.* 2021; Ma *et al.* 2019). We therefore  
 368 adopted ShB despite its large volume change during phase changes that required encapsulation of  
 369 its sheaths as a confined container.

370 When the results of Table 4 were scrutinised, ShB's absolute value of  $\Delta H$  was found to  
 371 be 42.73 J·g<sup>-1</sup>, which is a quarter of a typical  $\Delta H$  of PCMs (150 to 260 J·g<sup>-1</sup>) in architectural  
 372 applications yet is also similar to that of a fatty-acid mixture (40 to 100 J·g<sup>-1</sup>), which was suitable  
 373 for human comfort (18 °C to 25 °C) (Floros and Narine, 2016; Nazari *et al.* 2021). This can be  
 374 attributed to different experimental conditions or methods, such as the heating and cooling rate or  
 375 the isothermal duration required to keep ShB frozen for a certain crystallization period, as  
 376 mentioned above. The DSC results for the absolute values of the  $\Delta H$  of the PCMs and specimens  
 377 were not significant. Nonetheless, the relative values used to rank the enthalpy were used to  
 378 determine how the flow rate of the core/shell affected the  $\Delta H$ ,  $C_p$ , and  $k$ .

379 To compare the thermal behaviour of each sample,  $C_p$ , and  $k$  were calculated from the  
 380 DSC results (Table 4). During the DSC cycles of heating and cooling, we assumed that the change  
 381 in the internal energy of the system resulted from the only heat transfer rate ( $\dot{Q}$ ) in a closed  
 382 environment under constant pressure. The value for  $\dot{Q}$  can be obtained from the first law of  
 383 thermodynamics:

$$384 \quad \Delta E_{\text{system}} = \Delta Q_{\text{in-out}} + E_{\text{generat}} \text{ (J)} \quad \text{Eq. (2)}$$

$$385 \quad Q = m C_v \Delta T \text{ (kJ}\cdot\text{s}^{-1}\text{)} \quad \text{Eq. (3)}$$

$$386 \quad \dot{Q} = \dot{m} C_p \Delta T \text{ (kJ}\cdot\text{s}^{-1}\text{)} \quad \text{Eq. (4)}$$

387 where  $m$  is the mass of the specimen,  $\dot{m}$  is the mass flow rate,  $C_v$  is the specific heat of constant  
 388 volume, and  $C_p$  is the specific heat at constant pressure. One of the heat-transfer mechanisms, the  
 389 heat transfer rate ( $\dot{Q}_{\text{cond}}$ ), can be obtained from Fourier's law:

$$390 \quad \dot{Q}_{\text{cond}} = -kA \frac{dT}{dx} \quad \text{Eq. (5)}$$

391 where  $k$  is the heat conductivity of a substance,  $A$  is an area perpendicular to the heat transfer  
 392 direction, and  $dT/dx$  is the temperature gradient.

393 We found that the higher flow rate of the core, the greater the  $\Delta H$ ,  $C_p$ , and  $k$ , which was  
 394 the opposite to the effect of sheath flow rate. When the flow rate of the sheath increased from 2.0

395 mL/h to 4.0 mL/h,  $k$  of A-1T/A-2T at the same concentration (15.0 wt%) decreased from 0.524  
396  $\text{W}\cdot\text{m}^{-1}\cdot\text{K}^{-1}$  to 0.242  $\text{W}\cdot\text{m}^{-1}\cdot\text{K}^{-1}$ . This tendency was consistent with other cases, such as B-1T (4.0  
397 mL/h) versus B-4T (3.0 mL/h) as well as B-2T (4.0 mL/h) versus B-3T (3.0 mL/h) at 17.5 wt%  
398 with different flow rates of the core (the former, 1.0 mL/h; the latter, 0.5 mL/h). In contrast to the  
399 shell, the flow rate of the core was proportional to the  $\Delta H$ ,  $C_p$ , and  $k$ , presumably contributing to  
400 the amount of PCM. However, in the DSC results, all samples were expected to improve the  $k$  of  
401 the CA shells, accompanied by other techniques detailed below.

402 The techniques involved in improving  $k$  in the fabrication of the porous PCM with carbon  
403 composites have been subjected to numerous studies. Liu *et al.* (2017) demonstrated the stability,  
404 reliability, and corrosion resistance of an expanded-graphite composite with adipic-succinic acid  
405 of a mass ratio of 7:3, a corresponding  $\Delta H$  of 206  $\text{J}\cdot\text{g}^{-1}$  and a  $T_m$  of 135 °C. An expanded-graphite  
406 composite of eutectic capric-palmitic-stearic acids with a mass ratio 79:15:6 also proved to be  
407 thermally stable even after more than 500 thermal cycles despite a  $T_m$  of 21.3°C and a freezing  
408 point of 19.0°C with  $\Delta H$  exceeding 127  $\text{kJ}\cdot\text{kg}^{-1}$  (Zhang *et al.* 2016). Expanded graphite with a  
409 porous structure and acid-treated, expanded-vermiculite-loading aluminium-oxide particles affects  
410 the adsorption of eutectic lauric-myristic-palmitic acids with a mass ratio of 55:30:15 and eutectic  
411 lauric-myristic-stearic acids with a mass ratio of 59.5:32.0:8.5 and results in an increase in  $k$  of the  
412 composite (Zhang *et al.* 2013; Wei and Li, 2017). In summary, the  $k$  of the shell can be  
413 supplemented when coated with carbonaceous solutions or covered with porous foams in or onto  
414 encapsulated PCM-CA fibres.

415 To measure the mass ratio of ShB and CA, TGA and DTG thermograms were made in a  
416 range of 300 °C to 500 °C as shown in Fig. 5 (a) and Table 5. ShB was thermally degraded from  
417 423.97 °C to 477.35 °C, peaking at 461.14 °C. It consisted mainly of four components (C18:1,  
418 C18:2, C16:0, C18:0), with the boiling point of C16:0 overlapping the degradation temperature of  
419 the CA electrospun fibres (Table 2). However, the ratio of palmitic acid (C16:0, 3.3% to 3.9%) and  
420  $\text{TiO}_2$  and ZnO additives in ShB was nearly imperceptible and they were excluded from the TGA  
421 results presented in this study. The major component of stearic acid (C18:0) in ShB could be  
422 distinguished from other fatty acids as well as the CA fibres. The ratio of sheath to core was  
423 approximately 77.5–80.0 to 16.2–13.2. We therefore inferred that the B-1 sample had the largest  
424 amount of ShB core and the least ShB was contained in the C-2 or C-1 sample. The ratio obtained  
425 from the TGA results was in agreement with the DSC results that show the highest  $C_p$  were found  
426 in B-1T (0.421  $\text{J}\cdot\text{g}^{-1}\cdot\text{K}^{-1}$ ), and the lowest ones in C-1 (0.111  $\text{J}\cdot\text{g}^{-1}\cdot\text{K}^{-1}$ ). Fig. 5 (b) and (c) represent  
427 the ratio of C18:1 and C18:2 at 300 °C and that of C18:0 at 400 °C on the left side of the enlarged  
428 thermograms, consistent with Table 5.

429

430 *Human-wearing tests through paired differences in skin temperature in contact with electrospun*  
431 *fibres with or without PCMs*

432 Not only was the heat-transfer rate at the fibre level analysed in this study, we also  
433 attempted to verify the difference between the heat-transfer capacity of dual-structured PCM-CA  
434 electrospun fibres and that of single-structure CA fibres applied to the human body. To increase  
435 the  $k$  of PCM, the skin and the sample had to be in close contact. We therefore needed to design a

436 new hood and protective mask as the existing ones were not suitable for the thermal conduction of  
437 PCMs. Specifically, existing D-level protective clothing could not be used because PCM  
438 performance is realised only when it comes into direct contact with the skin. Fig. 6 (a) shows the  
439 new mask hood, which is divided into a head mask and a mask covering the face. The pieces of the  
440 mask hood were connected from the sideline of the ears, and heat could be easily dissipated by  
441 providing a large opening from the bottom of the back of the head. Velcro attached to the back  
442 functioned in two roles, not just opening but also adjusting in size. The electrospun fibre samples  
443 were then cut into  $10 \times 5 \text{ cm}^2$  pieces (total surface area:  $200 \text{ cm}^2$ ) and attached to the inside of the  
444 face hood onto the skins of forehead, cheeks, neck, and left chest, as shown in Fig. 6 (a). This  
445 pattern for the mask hood was produced using a human face-head model that was 3D-scanned and  
446 -printed.

447 The electrospun CA samples and PCM-CA samples were attached to the inside of the  
448 forementioned face hood and worn by six subjects to evaluate the change in skin temperatures at  
449 13 sites on their bodies. As shown in Fig. 6 (b), 75-min experiments were conducted twice per  
450 subject in a high-temperature and high-humidity environment ( $33 \text{ }^\circ\text{C}$ , 70% relative humidity). All  
451 the subjects sat to get accustomed to the environment for 35 minutes, then changed their hood.  
452 Next, after walking at 5 km/h on the treadmill for 20 min, they sat again and rested for 15 minutes.  
453 With the collected data of skin temperature and sweat, we found a significant difference in the  
454 effect of PCM cooling performance by comparing the skin temperature at the 13 sites, including  
455 the inner ear, with a paired t-test using SPSS.

456 Table 6 and Fig. 7 show the results of the paired t-test of the six subjects and the changes  
457 in skin temperature in the presence and absence of PCM in electrospun CA samples in the face  
458 hood. In Table 6, the mean skin temperature of individual subjects and the mean skin temperature  
459 of all six subjects were calculated by Eq. (1) from Hardy and Dubois, for comparison purposes.  
460 The mean skin temperature was lower when wearing a hood with PCM-CA electrospun fibres,  
461 except for subject B, whose mean skin temperature when wearing a hood without PCM in CA  
462 fibres was higher ( $34.650 \text{ }^\circ\text{C}$ ) compared with a hood with PCM in CA fibres ( $34.157 \text{ }^\circ\text{C}$ ).

463 Fig. 7 illustrates the differences in the average mean skin temperature of all six wearers in  
464 the presence and the absence of PCM in CA fibres of the mask hoods. The difference in skin  
465 temperature for each of the four sections at 1–20 min, 20–35 min, 40–60 min, and 60–75 min was  
466 analysed according to the experimental protocol. In Fig. 7, the black dotted line is the temperature  
467 when the hood without PCM was worn, and the red dotted line is the temperature when the hood  
468 with PCM was worn. Regardless of the presence or absence of PCM, the auditory canal  
469 temperature was approximately  $2 \text{ }^\circ\text{C}$  higher than the mean skin temperature, and it increased at a  
470 moderate rate. In the first recovery period at the beginning of the experiment, the temperature  
471 showed a constant or slight drop at 30 to 35 min during the initial stage of walking. This  
472 phenomenon could be a result of temporary cardiovascular contraction caused by sitting and  
473 walking. After changing to the second hood with the new PCM-CA samples, most subjects  
474 experienced a more gradual ascent in mean skin temperatures, and the difference between the  
475 hoods with and without PCMs had increased. The average skin temperature of all subjects was  
476 higher when wearing the hood with the PCM-CA fibres (emerald dotted line) by about  $0.20 \text{ }^\circ\text{C}$ ,

477 compared with the PCM in CA fibres (orange solid line). The average of mean skin temperatures  
478 was further delayed toward the second half of the experiment by increasing the gap to 0.25 °C at  
479 70–75 min compared with wearing a hood with the no PCM-CA fibres. This is in agreement with  
480 previous research that clothing made of the PCM-microcapsules and PCM-yarns dropped  
481 microclimate and humidity within the clothing (Bartkowiak *et al.* 2013). It was therefore  
482 concluded that PCM-CA fibres can help prevent skin temperature from increasing.

483 Another notable finding was the superior effectiveness of heat transfer as measured by the  
484 human-wearing assessment compared with the DSC results. The heating system in humans,  
485 metabolism, is different from the furnaces used in DSC and TGA and is associated with different  
486 thermoregulating mechanisms of homiotherms or isovelocities. The furnace was required to be  
487 set for a constant rate of heating and cooling, which meant more heat was available, to the point  
488 that it exceeded the latent heat of ShB, which then tried to react endothermically. This explains  
489 why the results of DSC and the human-wearing assessments were incongruent. Hou *et al.* (2019)  
490 contended that the most effective technique for evaluating protective clothing of PCMs is human-  
491 wearing assessment despite its high cost and time commitment. Mechanical techniques aided by  
492 software are designed to control process parameters based on mathematically simplified modelling  
493 but can cause difficulties when applied to human heat transfer, which organically intertwines the  
494 exchange of thermal conduction and convection from metabolic production to respiration, tissues,  
495 and blood (Hou *et al.* 2019). The basal metabolic rate (84.0 to 86.6 J·s<sup>-1</sup>) for the average male adult  
496 (30-year-old, 70 kg in weight, 173 cm in height, with a body surface area of 1.8 m<sup>2</sup>) increased by  
497 15 kcal·min<sup>-1</sup> during exercising compared to 0.5 kcal·min<sup>-1</sup> while sleeping, and lost 244 kJ of heat,  
498 corresponding to a decrease in body temperature of 1 °C as the  $C_p$  of human body is 3.49 kJ·kg<sup>-1</sup>·  
499 °C<sup>-1</sup> (Kenny *et al.* 2017; Yunus 2003).

500 Another difference between the DSC results and those of the human-wearing assessment  
501 was the change in  $k$  of the CA fibres by sweating. During the experiments, the subjects expressed  
502 considerable amounts of perspiration, which countered the increasing skin temperatures, consistent  
503 with other literature suggesting that releasing sweat or moisture increases heat capacity and storage  
504 by expanding the gap of  $k$  between materials and sweat (Raccuglia *et al.* 2017; Guan *et al.* 2020).  
505 Sweating could provoke evaporative cooling through the difference in water vapor pressures  
506 between the skin and the air. However, this study excluded the effect of convection by  
507 manipulating the ventilation and humidity of the experimental environment to make it windless-  
508 damp (relative humidity 70%).

509 To take advantage of complex mechanisms of heat transfer in humans, some researchers  
510 have attempted human-wearing trials of an innovative hybrid cooling system by means of the  
511 combination of thermal conduction, convection and irradiation. Hybrid cooling applications with  
512 PCMs, through wearing tests for eight subjects, were suggested with insulation layers, four fans in  
513 a cooling vest containing ice packs through heat convection and conduction (Chaen *et al.* 2019;  
514 Udayraj *et al.* 2019). Using ventilation fans lowered body core temperatures by 0.2°C and  
515 decreased rectum temperature by 0.13 °C and mean skin temperature near the neck by 5 °C. In  
516 sum, the cooling performance of PCM-CA electrospun fibres can be enhanced by adding an extra  
517 cooling apparatus in combination with thermal convection and irradiation.

## 518 **Conclusions**

519 Protective clothing for COVID-19 medical workers in hot, humid environments should  
520 incorporate thermoregulating mechanisms of heat transfer. To control heat transmittance of skin  
521 temperature, ShB composed of stearic and oleic acids was chosen for the PCM because of its  
522 appropriate  $T_m$  of 28 °C to 35 °C, bactericidal activity, and non-toxicity on human skin.

523 This research focused on the formation of electrospun CA fibres and PCM-CA fibres and  
524 their characterisation, heat capacity at measured by DSC and TGA analyses, and heat transfer  
525 through human body assessment. First, to fabricate the PCM encapsulation of a core-sheath  
526 structure, CA solutions of 17.5 wt% to 25.0 wt% were coaxially electrospun at a solvent ratio of  
527 A:D 1:1 from a TCD of 12 cm at the flow rate of 2.0 to 4.0 mL/h (sheath) and 0.5 to 1.0 mL/h  
528 (core). The morphology of PCM-CA electrospun fibres were characterised by the insertion of the  
529 core in sheath-like blood in tubular vessels with a few spherical beads as observed through TEM,  
530 SEM, and optical microscopy.

531 Second, DSC results revealed that the heat capacity of electrospun PCM-CA fibres was a  
532 half to a quarter of that of ShB, with a  $\Delta H$  of 42.73 J·g<sup>-1</sup>, a  $C_p$  of 1.90 J·g<sup>-1</sup>·K<sup>-1</sup> and  $k$  of 1.407  
533 W·m·K<sup>-1</sup>. The sheath flow rate was inversely proportional to the heat capacity of the PCM-CA  
534 fibres, as measured by  $\Delta H$ ,  $C_p$ , and  $k$ . This can be attributed to the thickness of the sheath wall,  
535 which corresponded to the flow rate of the sheath. In contrast to the flow rate of the sheath, the  
536 relationship between the flow rate of the core and the heat capacity was proportional. In TGA  
537 results, the thermal degradation peak of ShB was 461.14 °C (due to its major component of steric  
538 acid) and that of CA was 389.61 °C a result of mixing with the palmitic acid. The ratio of CA to  
539 ShB was inferred to be as high as 78% to 80% and as low as 16% to 13%. The electrospun PCM-  
540 CA fibres with the highest ratio of ShB as shown in TGA coincided with the fibres with the largest  
541  $k$  of 0.421 J·g<sup>-1</sup>·K<sup>-1</sup> in the DSC results.

542 Finally, in the human-wearing assessment, wearing a hood with PCM-CA fibres (the  
543 experimental condition) decreased mean skin temperature in five of six subjects by 0.5 °C,  
544 compared to attaching only CA fibres (the control). During the walking exercise, the difference in  
545 the two conditions gradually rose to 0.25 °C. At 70–75 min during the second sitting-rest after  
546 walking, the average mean skin temperatures sharply dropped, resulting in the biggest gap between  
547 the two conditions, as supported by the paired t-test ( $p < 0.05$ ). In conclusion, the effectiveness of  
548 PCM-CA fibres was validated as it delayed the increase of skin temperatures.

549 This study successfully encapsulated PCM by coaxially electrospinning a core-sheath  
550 structure. It was also confirmed the potential of the technique for thermoregulating protective  
551 clothing. We found it is necessary for the core to increase latent heat as well as for the sheath to  
552 enhance  $k$ . For this, future research should address the fabrication of PCM composites by coating  
553 them with carbonaceous materials to improve heat transfer through the combination of thermal  
554 conduction and convection.

555

556

557

558 **Acknowledgements**

559 I would like to thank my research colleagues and professor Sohyun Park at the Korea national  
560 open university for providing electrospinning apparatus and staffs of NanoNC for advising  
561 experiments and their helps.

562 **Author's Contributions**

563 Conceptualisation, experiments, analyses, investigation, data curation, writing, review and editing,  
564 visualization, Hye Jin Kim; supervision, funding acquisition, Changsang Yun; consultation, Ji Hun  
565 Park; preparation of human wearing tests, Syifa Salsabila.

566 **Conflict of interest**

567 We are pleased to declare no conflict of interest.

# Figures

## Figure 1

Schematic diagram of total experiments in this research

## Figure 2

SEM and optical microscopic images of 25.0 wt% electrospun CA fibers in A:D 1:1 (v/v) solvents (a) a histogram and optical microscopic image of the CA fibre (magnification: 4x), (b) SEM image of the CA fibre (magnification: 200x, SE), (c) optical microscopic image of the CA fibre (magnification: 10x), (d) SEM image of the CA fibre (magnification: 5x, SE)

## Figure 3

TEM images of encapsulation of PCM as a core in CA electrospun fibers as sheaths (a) two concentric Taylor cones of core-sheath solutions, (b) enlarged TEM image of ShB core encapsulated in sheath CA fibre, (c) SEM image of the ShB encapsulated in CA fibres, (d) enlarged TEM image of the ShB-CA fibre

## Figure 4

DSC results for shea-butter, coconut oil and PCM-CA fibers in (a) heating and (b) cooling

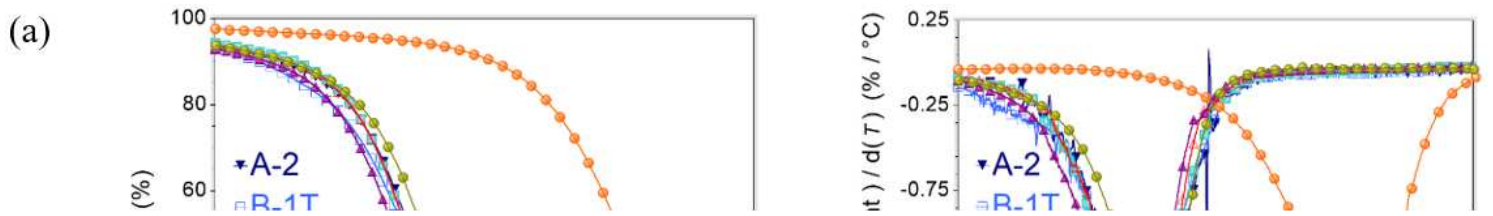


**Figure 5**

TGA results for shea-butter and PCM-CA fibers in a range of (a) 300 °C to 500 °C, (b) 300 °C to 400 °C and (c) 380 °C to 480 °C

**Figure 6**

(a) Schematic designs of face-hoods for human wearing assessment and attachment sites for electrospun fibers with and without PCM, (b) experimental protocols and (c) IR thermal and photographic images during the human wearing assessment

**Figure 7**

Changes in mean skin temperature and auditory canal temperature of all subjects according to the presence of PCM or absence of the PCM (control condition) in CA fibers of face-hoods

## Supplementary Files

This is a list of supplementary files associated with this preprint. Click to download.

- [groupimage1.png](#)